Membrane Potential and Human Erythrocyte Shape

Margaret M. Gedde and Wray H. Huestis
Department of Chemistry, Stanford University, Stanford, California 94305 USA

ABSTRACT Altered external pH transforms human erythrocytes from discocytes to stomatocytes (low pH) or echinocytes (high pH). The process is fast and reversible at room temperature, so it seems to involve shifts in weak inter- or intramolecular bonds. This shape change has been reported to depend on changes in membrane potential, but control experiments excluding roles for other simultaneously varying cell properties (cell pH, cell water, and cell chloride concentration) were not reported. The present study examined the effect of independent variation of membrane potential on red cell shape. Red cells were equilibrated in a set of solutions with graduated chloride concentrations, producing in them a wide range of membrane potentials at normal cell pH and cell water. By using assays that were rapid and accurate, cell pH, cell water, cell chloride, and membrane potential were measured in each sample. Cells remained discoid over the entire range of membrane potentials examined (−45 to +45 mV). It was concluded that membrane potential has no independent effect on red cell shape and does not mediate the membrane curvature changes known to occur in red cells equilibrated at altered pH.

GLOSSARY

Nomenclature

a_{Cl}	activity of chloride
^{36}Cl	^{36}Cl dpm
Cl_{tot}	total cell chloride (fmol)
[Cl]	chloride concentration (molar)
cw_o	normal cell water (pg)
Fr	fraction
Hb	hemoglobin
$[Hb]_o$	normal cell hemoglobin concentration
in	intracellular
K	activity gradient, Donnan ratio
M	mass
O	osmoles (osmol)
$O_{c,\,ref}$	osmoles of reference cells (fosmol)
$O_{Hb,\,ref}$	hemoglobin osmoles of reference cells (fosmol)
Os	osmolality (osmolal)
out	extracellular
p	pellet
pw	pellet water
r	concentration gradient
ref	reference
s	supernatant
sol	cell solids
tw	trapped water
V	volume

Greek

γ_{Cl}	activity coefficient of chloride
$\Delta\Psi$	membrane potential (mV)
ρ	density
ϕ_{Hb}	hemoglobin osmotic coefficient

Received for publication 28 September 1994 and in final form 3 December 1996.

Address reprint requests to Dr. Wray H. Huestis, Department of Chemistry, Stanford University, Stanford, CA 94305. Tel.: 415-723-2503; Fax: 415-723-4817; E-mail: hf.whu@forsythe.stanford.edu.

Dr. Gedde's present address is Department of Pathology and Laboratory Medicine, University of Pennsylvania Medical Center, Philadelphia, PA 19104.

0006-3495/97/03/1220/14 $2.00

INTRODUCTION

The normally smooth, discoid membrane of the human erythrocyte is transformed by a variety of chemical and physiological treatments into stably invaginated and evaginated forms (stomatocytes and echinocytes). Because the mammalian erythrocyte has no internal cellular structure, the changes in membrane topology must result exclusively from changes in forces originating within the membrane itself. The study of shape transformations and other erythrocyte characteristics has yielded a wealth of mechanical and molecular data, making the erythrocyte membrane the best characterized of biological membranes (Elgsaeter et al., 1986; Steck, 1989; Berk et al., 1989; Bull and Brailsford, 1989; Shen, 1989; Liu and Derick, 1992).

The mechanisms of several observed shape transformations have been explained satisfactorily, including those involving intercalation of exogenous compounds into the lipid bilayer (Sheetz and Singer, 1974; Fujii et al., 1979; Ferrell et al., 1985; Daleke and Huestis, 1989) and change in native lipid composition and distribution (Ferrell and Huestis, 1984; Lin et al., 1994). However, major sets of shape change observations still cannot be understood in terms of current molecular models (for example, Lovrien and Anderson, 1980; Jinbu et al., 1984; Raval et al., 1989), suggesting that significant features of the membrane assembly remain undescribed.

It is well known that red cells undergo pH-dependent shape transformations, and that, unlike most described shape changes, they proceed readily at room temperature. The classic "glass effect" (echinocytosis of washed red cells placed in contact with glass) depends on the elevation of extracellular pH (Furchgott and Ponder, 1940; Trotter, 1956; Weed and Chailley, 1973). In an electrical field, red cells echinocytose near the cathode and stomatocytose near the anode; the shape changes correlate, respectively, with high and low local pH, and are reproduced by spraying cells with dilute base or acid (Rand et al., 1965). Red cells placed

directly into high- or low-pH buffers become echinocytes and stomatocytes, respectively (Weed and Chailley, 1973). These pH-associated shape changes occur in seconds upon alteration of the extracellular environment, and reverse in seconds when the environment is normalized. Reversibility has been demonstrated most strikingly for transformations induced by application and reversal of an electrical field (Rand et al., 1965) and approach and withdrawal of a glass rod (Bessis and Prenant, 1972); in the latter case, glass echinocytosis of individual cells could be induced and reversed almost indefinitely. The speed and reversibility of pH-associated shape changes make it unlikely that they are mediated by disruption of covalent or high-affinity linkages. Rather, data are consistent with low-energy shifts in weak, noncovalent bonds. In this model, pH-dependent changes in electrostatic and/or hydrophobic linkages within the native membrane would produce mechanical imbalances and altered shape. Information about pH-dependent structures in red cell membranes could be applicable to biological membranes in general.

However, the molecular mechanism of pH-associated shape change has remained obscure. Two separate factors compound the puzzle. First, a proposed comprehensive model of erythrocyte shape determination (Elgsaeter et al., 1986) does not predict the observed effects of pH on red cell shape. Strong dependence of spectrin gel tension on pH is predicted to cause the membrane skeleton to contract at low pH and expand at high pH, producing echinocytosis and stomatocytosis, respectively. This predicted effect is opposite that observed. Second, it cannot be assumed that cell (i.e., interior or cytosolic) pH is the physiological property mediating cell shape change in altered pH solutions. Alteration of external pH causes strong simultaneous shifts in cell pH, membrane potential, cell chloride, and cell water (Jacobs and Stewart, 1947), all of which correlate with the changes in membrane curvature.

The findings of Glaser and co-workers provide a possible solution to this puzzle. They have reported that erythrocyte membrane potential mediates pH-induced shape change (Glaser, 1979, 1982; Glaser et al., 1980, 1987, 1988, 1991; Glaser and Donath, 1984, 1989). This might explain why the predictions of the model of Elgsaeter and co-workers, which did not consider membrane potential, differ from the experimental observations. However, Glaser's reports do not present control experiments excluding roles for the other cell properties that vary when external pH is changed. Moreover, other workers have found no effect of membrane potential on red cell shape (Bifano et al., 1984).

The aim of this study was to demonstrate unambiguously the presence or absence of an independent membrane potential effect on red cell shape. Red cells were equilibrated in a set of solutions with graduated chloride concentrations, producing in them a wide range of membrane potentials at normal cell pH and cell water. Over the range −45 to +45 mV, membrane potential was found not to be an independent mediator of red cell shape.

MATERIALS AND METHODS

Reagents

Chemicals were purchased as follows: 2-[*N*-morpholino]ethanesulfonic acid (MES), HEPES, 2-[*N*-cyclohexylamino]-ethanesulfonic acid (CHES), glutaraldehyde (EM Grade), and [^{14}C]methoxy-inulin from Sigma (St. Louis, MO); Na^{36}Cl and EcoLite scintillation fluid from ICN Biomedicals (Irvine, CA); and NCS Solubilizer from Amersham/Searle (Arlington Heights, IL). Other chemicals were at least reagent grade.

Red cells

Venous blood was obtained from normal adult donors, and citrate was used as the anticoagulant. Red cells were separated from white cells and plasma by centrifugation, washed three times with three volumes of 0.15 M sodium chloride, and suspended at 20% Hct in 138 mM sodium chloride, 5 mM potassium chloride, 7.5 mM sodium phosphate, 1 mM magnesium sulfate, and 5 mM glucose at pH 7.4 (PBS). Cells not used immediately were stored in PBS at 5°C.

The morphology of cell preparations was checked before using them in experiments. Freshly washed cells were slightly stomatocytic; one or more hours in PBS at room temperature restored discoid morphology. Cells stored overnight became slightly crenated; these were restored to discs by a 15-min 37°C PBS incubation. All cells were used within 18 h of drawing.

A starting morphological index (MI) of −0.10 to +0.03 (see below) was accepted as normal.

Preparation of experimental solutions

Experimental solutions contained a range of concentrations of potassium chloride plus sufficient sucrose and/or potassium gluconate to maintain constant osmolality within experiments (Fig. 8). In early experiments, sucrose was the osmotic supplement; in later experiments, potassium gluconate was preferred in low chloride solutions (especially with high pH cells) to slow leakage of cell salts (Gedde et al., 1997). Buffered solutions also contained MES, HEPES, or CHES.

Sucrose and potassium gluconate concentrations predicted to produce target osmolalities at specific potassium chloride and buffer concentrations were calculated as required: supplemental osmolality divided by osmotic coefficient. Supplemental osmolality was calculated by subtracting potassium chloride and buffer osmolality from total target osmolality. Osmotic coefficients of potassium chloride and potassium gluconate (assumed to be concentration independent) were 1.8 (Wolf et al., 1978) and 1.65 (experimental result), respectively. Sucrose osmotic coefficient as a function of concentration was calculated from published data (Wolf et al., 1978). Buffering compound osmotic contribution was calculated as the product of the estimated buffer osmotic coefficient, 0.9 osmolal/molar particles, and total particle concentration (Particle, molar); particle concentration was calculated from salt and acid-base chemistry as a function of pH and buffer concentration (Conc, molar):

$$\text{Particle} = \text{Conc}\left(1+\left(\frac{10^{K}}{1+10^{K}}\right)\right), \qquad (1)$$

where K = pH − buffer pK_a. Buffer concentration was usually 50 mM, with a minimum concentration of 20 mM. Solutions constructed by this procedure typically had measured osmolalities within 3% of target osmolalities.

Equilibration of cells in experimental buffers

For experiments in which cell pH was to be altered significantly (Figs. 1 and 2), cells were brought to the new electrochemical equilibrium state by repeated room temperature equilibration in experimental buffer. Cells were suspended in the appropriate buffer at 10% Hct and incubated for 5–10 min

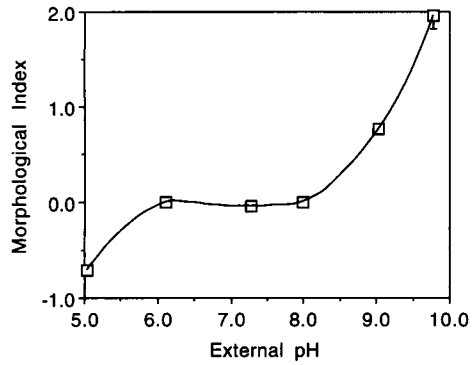

FIGURE 1 Effect on erythrocyte shape of equilibration in altered pH buffers. Cells were equilibrated in buffers containing 100 mM potassium chloride, 20 mM potassium gluconate, and 50 mM MES (points near pH 5 and 6), HEPES (points near pH 7 and 8), or CHES (points near pH 9 and 10). Morphology was assessed as described in Materials and Methods. Error bars represent standard deviations; error bars that are not visible are smaller than the plot symbols. The line is a computer interpolation of the data.

at room temperature. In this incubation, transmembrane redistribution of chloride and hydroxide (and equivalently, protons) via the anion exchanger changed the pH of both the cytosol and the external buffer. Preliminary experiments showed that the new equilibrium was reached in 5–10 min, depending on the strength of the buffer and the increment between the initial and final equilibrium states. The resuspension/incubation cycle was repeated until cells no longer changed the pH of the external buffer (i.e., suspension pH remained stable at the same value as that of the prepared experimental buffer). Three to five cycles were usually required. Electrochemical equilibrium as reflected in the stability of suspension pH (±0.02 pH units) was verified for each sample in all experiments. By allowing time for full pH equilibration via the anion exchanger, use of proton ionophores (Macey et al., 1978) was avoided.

Membrane potential series experiments

To alter membrane potential without affecting cell pH, cells were placed in a series of unbuffered solutions containing decreasing concentrations of potassium chloride, plus sucrose or potassium gluconate sufficient to keep

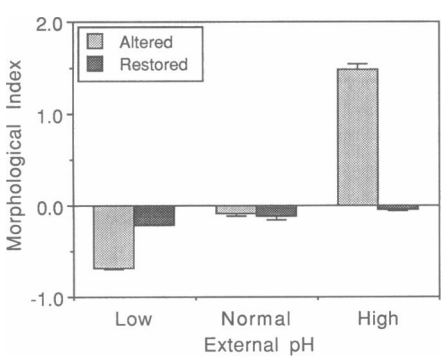

FIGURE 2 Reversibility of erythrocyte shape change occurring in altered pH buffers. Cells were equilibrated in buffers containing 100 mM potassium chloride, 40 mM sucrose, and 50 mM MES, HEPES, or CHES at pH 5.0, 7.5, and 9.8, respectively, and morphology was assessed. Samples were then equilibrated in 100 mM potassium chloride, 50 mM sucrose, 50 mM HEPES at pH 7.5, and the morphology was again assessed. ▨, Altered pH morphology. ■, Morphology after restoration of normal pH.

osmolality constant. However, buffered cell suspensions were required for assessment of morphology and external pH (procedures described below). Therefore, sets of buffered solutions containing the same potassium chloride concentrations as the unbuffered solutions plus 20 mM buffer (usually HEPES) and compensating sucrose or potassium gluconate also were prepared. In each experiment, cells were washed once and resuspended at 10% Hct in the unbuffered solutions. The pH of each unbuffered suspension was measured directly (Macey et al., 1978). Then the pH of each buffered solution was adjusted to the pH of its matched suspension, and samples were resuspended at 10% Hct in the matched buffers. After 10 min of equilibration, samples were assayed for morphology and four cell properties (cell pH, membrane potential, cell chloride, and cell water).

Elevation of 2,3-diphosphoglycerate

For some experiments, cells were equilibrated in inosine-pyruvate-phosphate buffer (80 mM sodium chloride, 10 mM inosine, 10 mM pyruvate, 5 mM glucose, and 50 mM sodium phosphate, pH 7.4; IPP buffer) and incubated at 37°C at 10% for 1–2 h. This elevated cytoplasmic 2,3-diphosphoglycerate to 15–25 mM, from normal levels of about 5 mM (Deuticke et al., 1971).

Morphology assay

To ensure that fixed morphology reflected that in the experimental buffers at equilibrium, cells were fixed in their own supernatant. Fix solutions contained 2 μl 25% glutaraldehyde and 250 μl supernatant from above the pelleted cells; into this was mixed 20 μl of 10% cell suspension, giving a final cell concentration of 0.7% and a final glutaraldehyde concentration of 0.2% (effective glutaraldehyde osmolality ~10 mosM; Hayat, 1981). This protocol provided a fourfold excess of the glutaraldehyde required to fix the samples completely (Morel et al., 1971). Because glutaraldehyde stocks are acidic, fix supernatants contained at least 20 mM buffer. Samples were fixed for 10 min or more, and morphology was assessed at 400× by bright-field light microscopy on glass slides.

Cell morphology was scored on a stomatocyte-echinocyte scale based on Bessis' nomenclature (Bessis, 1973; Ferrell et al., 1985; Daleke and Huestis, 1989) with discocytes scored as 0. The criteria used were as follows. Flattened or elongated cells with spikes were scored as stage +1 or +2, whether the spikes were broad or fine, with number of spikes distinguishing stages +1 and +2. Stage +3 cells were rounded with broad spikes; stage +4 cells were round with fine spikes; and stage +5 cells were smooth spherocytes. Stage −1 stomatocytes had one large invagination, with no remaining trace of biconcavity. Stage −2 cells had one main invagination with additional smaller ones, or several small invaginations exclusively on one side of the cell. Stage −3 cells had evenly distributed small invaginations, and stage −4 cells were smooth spherocytes. Special attention was given to distinguishing discocytes and stage −1 stomatocytes viewed from above. In our preparations, the indentations of discocytes had gradually sloping edges. The stomata of stomatocytes had more sharply defined edges. The shapes were distinguished by focusing up and down through the cells.

The morphological index (MI) was the average of 100 scores. MI was determined at least in duplicate for each sample. Replicate determinations for individual samples were performed nonconsecutively. The experimental condition being observed was unknown at the time of assessment. Standard deviations were less than 0.15 MI unit for nearly all samples.

pH measurement

Supernatant and pellet lysate pHs were measured with a miniature combination pH electrode (Ag/AgCl reference, ceramic liquid junction; Ingold Electronics, Wilmington, MA) and PHM 82 standard pH meter (Radiometer, Copenhagen, Denmark). Lysate readings were allowed to stabilize fully, to minimize the possible effects of liquid junction potentials (Westcott, 1978).

Cell pH samples were prepared by pelleting 1.5 ml 10% cell suspension for 5 min at 13,600 × *g*. Greater exclusion of trapped supernatant by firmer packing did not change measured pH values. Supernatant aliquots were retained, and the remaining supernatant and the top cell layer were aspirated. Pellets were freeze-thaw lysed (three cycles), and their pH was measured at room temperature. Samples in which pH was not measured immediately were stored at −20°C; storage for even 12 h at 5°C resulted in acidification of the samples, presumably from glycolytic production of lactic acid. Replicate samples rarely differed by more than 0.02 pH units.

Calculation of membrane potential

Application of the Nernst equation at room temperature gave

$$\Delta\Psi(\text{mV}) = -59(\text{pH}_{\text{out}} - \text{pH}_{\text{in}}), \tag{2}$$

where pH_{out} = supernatant pH and pH_{in} = measured cell pH. Standard deviations were less than 2 mV for nearly all samples.

Gravimetric cell water assay

In tared 1.5-ml microcentrifuge tubes, 0.15 ml of cells in 10% suspension were pelleted for 15 min at 8800 × *g* in a centrifuge giving pellets flattened perpendicular to the tube axis (diameter of top of pellet, 6 mm; diameter of bottom of pellet, 2 mm). Supernatant aliquots were retained for chloride and osmolality determinations. Remaining supernatant and the top layer of cells were removed by aspiration, and moisture was removed from the cap and walls of the tube with a cotton swab. Tubes were capped and weighed, uncapped and dried at 70–90°C to constant mass (about 50 h), and reweighed after cooling for 30 min in a desiccator.

Average cell water content was calculated from

$$\text{Cell water (pg)} = 36\left(\frac{W - D}{D - T}\right), \tag{3}$$

where T is the tube tare weight, W is the weight of tube plus fresh cell pellet, D is the weight of the tube plus dried pellet, and 36 ± 1 pg/cell was determined by hemacytometer to be the dry mass per cell. Determinations in duplicate or triplicate yielded standard deviations of less than 1.5 pg for nearly all samples. All cell water assay results were corrected for the presence of trapped supernatant (Appendix B).

In samples in which membrane potential was determined from the distribution of ^{36}Cl (Appendix A), the following values were also calculated:

$$\text{Pellet mass } (M_p) = W - T \tag{4}$$

$$\text{Pellet water mass } (M_{pw}) = W - D \tag{5}$$

$$\text{Pellet solids mass } (M_{sol}) = D - T \tag{6}$$

$$\text{Water mass fraction } (M\text{Fr}_{pw}) = \left(\frac{W - D}{W - T}\right). \tag{7}$$

Rapid assay of cell volume

As a supplementary, rapid means of assessing cell water, a cell volume assay was employed. To assay cell volume rapidly, 20 μl experimental cell suspension at 10–20% Hct was combined with 1 ml 0.02% Triton X-100 and 2 ml Drabkin's reagent (20 mg% $K_3Fe(CN)_6$, 5 mg% KCN, 100 mg% $NaHCO_3$). Absorbance at 540 nm relative to water was determined. The hematocrit of the suspension was determined simultaneously, and Hct-to-A_{540} ratios for experimental and normal cells were compared. This assay provided same day assessment, but lacked the precision of the gravimetric assay for cell water.

Chloride assay

Chloride concentration in the final supernatant of each equilibrated cell suspension was determined by mercurimetric titration (Schoenfeld and Lewellen, 1964). Color reagent and reagent blank solutions were prepared as described and stored in the dark. The molarity of potassium chloride standard solutions was calculated from measured osmolality and published tables (Wolf et al., 1978). Sample (20 μl) plus color reagent or reagent blank (2.0 ml) were mixed in assay tubes, and absorbance in color versus blank tubes was measured at 450 nm after 10 min. Individual sample blanks were required because of interference at 450 nm by some buffer components. When chloride concentrations above 50 mM were assayed, 6 or 12 μl saturated $Hg(NO_3)\cdot H_2O$ (quench reagent) was added per 5.0 ml blank or color solution to reduce assay sensitivity. Sample chloride concentrations were calculated from standard curves run at each level of quench. Standard deviations were typically 3 mM or less.

Calculation of cell chloride concentration

From Eq. A3 (Appendix A),

$$[\text{Cl}]_{\text{in}} = \left(\frac{\gamma_{\text{Cl}_{\text{out}}}}{\gamma_{\text{Cl}_{\text{in}}}}\right)[\text{Cl}]_{\text{out}}\, e^{(\Delta\Psi/25.5)}. \tag{8}$$

Because γ_{Clin} itself depends on $[\text{Cl}]_{\text{in}}$ (Eq. A14), Eq. 8 was solved by iteration using Cl_{out} and $\Delta\Psi$. Total cell chloride was calculated by multiplying cell chloride concentration and cell water (trapping corrected).

Osmolality

Osmolality was measured on a model 5000 vapor pressure osmometer (Wescor, Logan, UT) calibrated using glass ampule-sealed standards (Wescor).

Determination of ^{36}Cl distribution

Experimental cells were pelleted from 1.5 ml 10% suspension, and most supernatant was removed. Approximately 0.1 μCi $Na^{36}Cl$ in 5 μl stock solution was added, and the cells were resuspended in the remaining supernatant. After 5 min of equilibration, the suspension was centrifuged (5 min, 13,600 × *g*), and 75 μl supernatant was combined with 2 ml EcoLite in scintillation vials. The remaining supernatant was removed, and 75 μl packed cells were pipetted into 20-ml scintillation vials. So that supernatant and packed cell sample volumes would be identical, the same positive-displacement pipette (model DV-100A; Labindustries/Barnestead Thermolyne, Dubuque, IA) on the same setting was used to deliver all samples.

Cell pellet samples were solubilized by adding 1 ml NCS solubilizer and heating for 20 min at 60°C. When cool, they were decolorized by adding 1 ml saturated benzoyl peroxide in toluene (prepared by heating 1 g benzoyl peroxide in 5 ml dry toluene for 10 min at 60°C and decanting the cooled solution). Chemiluminescence resulting from the presence of benzoyl peroxide was minimized by neutralizing samples with 100 μl of glacial acetic acid and heating samples at 60°C for 1 h. After cooling, 9 ml EcoLite was added, and samples were stored in the dark for several days until chemiluminescence approached background.

Disintegrations per minute in all samples were determined between 200 and 860 meV in a Beckman (Irvine, CA) LS3801 scintillation counter using a ^{36}Cl quench curve, until the standard error was less than 0.25% of the result.

As described in Appendix A, membrane potential was calculated using pellet and supernatant ^{36}Cl dpm. Because volumes of pellet and supernatant samples were equal, their values were not required for this calculation.

Computations

Calculations were performed using standard statistical procedures (Skoog, 1985). Figure error bars represent standard deviations.

RESULTS

Effect of altered external pH on red cell morphology

Equilibration in buffers of pH 5.0 to 9.8 at constant chloride concentration and osmolality transformed human erythrocytes from discocytes to stomatocytes (low pH) and echinocytes (high pH), with morphological indices (MIs) of -0.71 ± 0.06 to $+1.96 \pm 0.14$ (Fig. 1). A similar experiment using cells from a different donor produced MIs of -0.92 ± 0.04 at low pH and $+2.44 \pm 0.19$ at high pH. The observed shape changes were readily reversed by reequilibration in normal pH buffers (Fig. 2).

Assays for physiological cell properties

Erythrocyte cell pH, cell chloride, cell water, and membrane potential are all known to vary when external pH is changed (Jacobs and Stewart, 1947; Freedman and Hoffman, 1979; Glaser and Donath, 1984). To distinguish among their roles in the accompanying shape change, rapid and accurate assays for these properties were developed.

Direct pH measurement in freeze-thaw lysed cell pellets was a simple, rapid, and precise method for determining cell pH (results with standard deviations of 0.02 pH units available in 30 min). (Measurement of the pH of diluted lysates is technically convenient; however, because proton activity depends on ionic strength (Westcott, 1978), and ionic strength in packed cell lysate is markedly different from that of diluted lysate, this is not expected to give accurate results. For example, in one experiment, a detergent lysis method (Semplicini et al., 1989) gave pHs differing from those of the freeze-thaw lysis method by as much as 0.35 pH units.) By using a pH electrode suitable for sample volumes of 100 μl, multiple samples could be processed. In comparison, determination of cell pH by the assessment of ^{36}Cl distribution is a time-consuming procedure involving complex manipulations, calculations, and assumptions (for example, see Freedman and Hoffman, 1979).

However, nonzero pH electrode liquid junction potentials that can arise in concentrated polyelectrolyte solutions (Westcott, 1978) might produce inaccuracies in direct pH measurements on packed cell lysates. Because such junction potentials arise only in the presence of net polyelectrolyte charge, no inaccuracy is expected near the cytoplasmic isoelectric point (about pH 6.8). To assess whether direct pH measurement of packed cell lysates was sufficiently accurate at cell pH extremes, it was compared to the ^{36}Cl method in two experiments (Fig. 3). Cell pH was calculated from ^{36}Cl data (Appendix A) and plotted against lysate pH values. At extremes of cell pH, the assays disagreed slightly. The maximum deviation from a line of slope 1 was 0.09 pH units, equivalent to a membrane potential difference of 5.3 mV. The differences could reflect either slight liquid junction potentials at pH extremes or pH-dependent variation in chloride activity coefficients (Pfister and Pauly, 1964). Because the deviation was minor and occurred only at extreme pH values, measured lysate pH was used as the cell pH in all experiments.

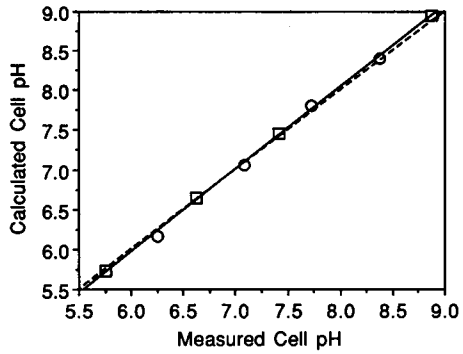

FIGURE 3 Comparison of measured lysate pH and cell pH calculated from 36-chloride ratios. Cells were equilibrated in altered pH buffers. Lysate pH, cell water, external chloride, and ^{36}Cl distribution were assayed as described in Materials and Methods, and cell pH was calculated from the ^{36}Cl distribution as described in Appendix A. Results from two experiments are shown. The dashed line has a slope of 1; the solid regression line represents the equation $y = -0.26 + 1.04x$.

Measurement of cell pH values permitted membrane potential and cell chloride to be determined relatively easily. Membrane potential was calculated by Eq. 2. Cell chloride was calculated from membrane potential and external chloride (Eq. 8). Cell water was assayed gravimetrically and corrected for intercellular trapping of supernatant in cell pellets (see Appendix B). No correction for "water of hydration" was made. (The usefulness of the concept of cell water of hydration (protein-bound, osmotically inactive water unavailable to solubilize salts) has been questioned, because the amount of water available to a solute probe depends on its size, steric configuration, and functional groups, and on temperature (Cook, 1967; Gary Bobo, 1967). The dependence of hemoglobin's osmotic coefficient on its concentration adequately explains red cell osmotic responses (Freedman and Hoffman, 1979).) Each assay except the cell water assay could yield same-day results, or could be stored (lysates and supernatants at $-20°C$) and completed at a later time. A preliminary cell water result could be obtained by using the rapid assay for cell volume.

To evaluate the accuracy of this system of assays, the buffering capacity of the cell was determined by calculating total cell chloride, plotting it against cell pH, and calculating the slope of this function (the buffering capacity) (Fig. 4). Because this calculation used all four of the assayed cell properties, it provided a check of the overall system. The buffering capacity between pH 6 and 8 was -11.9 (equiv) $(\text{mol Hb})^{-1}(\text{pH unit})^{-1}$, in reasonable agreement with a prior report of -12.6 (Freedman and Hoffman, 1979). The titration curve of hemoglobin, which this buffering curve should reflect, is shown superimposed on the data points.

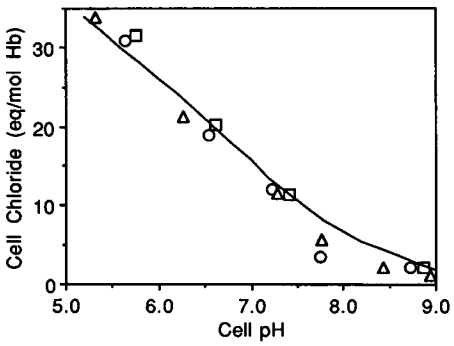

FIGURE 4 Dependence of total cell chloride on cell pH. Cell chloride concentration was calculated from external chloride and membrane potential, and total cell chloride from cell chloride concentration and cell water, as described in Materials and Methods. Data from three separate experiments are shown. The titration curve of hemoglobin (Antonini and Brunori, 1975) is superimposed over the cell chloride data.

Physiological changes occurring when external pH is altered

To demonstrate the known physiological effects of altered external pH on cell pH, cell chloride, cell water, and membrane potential (Jacobs and Stewart, 1947; Freedman and Hoffman, 1979; Glaser and Donath, 1984), the samples described in Fig. 1 were assayed for these four physiological variables. Results are shown in Fig. 5. Variation of external pH from 5.0 to 9.8 at constant chloride and osmolality produced a cell pH of 5.3 to 8.9 (normal, 7.2); a membrane potential of +17 to −50 mV (normal, −10 mV); cell water of 88 to 48 pg (normal, 67 pg); and a cell chloride concentration of 197 to 12 mM (normal, 85 mM). Thus, low cell pH, positive potential, high cell water, and/or high cell chloride were stomatocytogenic; and high cell pH, negative potential, low cell water, and/or low cell chloride were echinocytogenic. Fig. 6 summarizes these relationships.

Correlation of membrane potential and cell shape: control for cell shrinkage

Previous reports correlate changes in membrane potential and red cell shape (Glaser, 1979, 1982). For example, cells placed at positive potential by equilibration in low chloride solutions were discoid; when shifted to negative potential through chloride redistribution upon the addition of cation ionophore, cells were echinocytic. It was concluded that the membrane potential shift caused the change in red cell shape. However, other physiological properties change in such treatments. With the addition of ionophore, significant amounts of cell chloride and cell water are lost, and the cytoplasm becomes acidified to an extent determined by the strength of the extracellular buffer.

The shape effects of shrinkage in this reported protocol were examined. Red cells were equilibrated in low chloride buffer at normal pH as described (Glaser, 1979). An aliquot was treated with nystatin to shift the membrane potential from positive to negative. This sample became both shrunken and echinocytic (Fig. 7, *filled circle*). Other aliquots were shrunken by exposure to excess sucrose. These shrunken cells were also echinocytic, although the membrane potential remained positive (Fig. 7, *open circles*). (Sucrose-shrunken cells were more echinocytic than nystatin-treated cells, consistent with our finding that nystatin is stomatocytogenic (Gedde et al., 1997).) Thus shape change

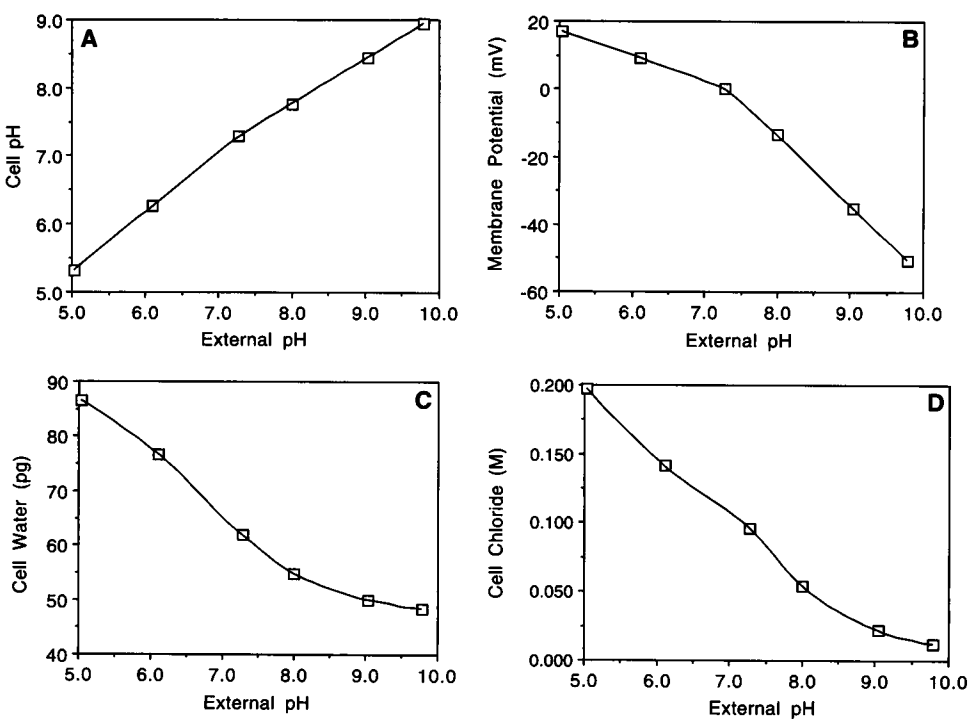

FIGURE 5 Changes in four cell physiological properties in cells equilibrated in altered pH buffers. Cell pH (*A*), calculated membrane potential (*B*), cell water (*C*), and calculated cell chloride concentration (*D*) were determined for the samples shown in Fig. 1. The data are representative of two other similar experiments. Error bars that are not visible are smaller than the plot symbols. The lines are computer interpolations.

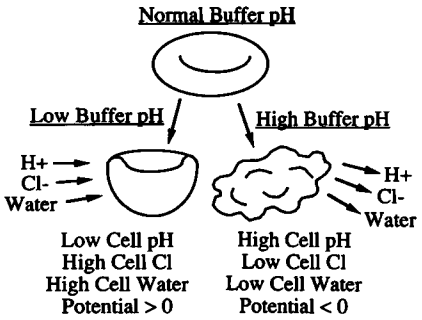

FIGURE 6 Change of red cell properties with altered external pH.

did not correlate with membrane potential change in this protocol.

Independent variation of membrane potential and effect on shape

To assess the effect of membrane potential on shape, the potential had to be varied independently, without simultaneous shifts in cell pH, cell chloride, or cell water. By lowering external chloride in unbuffered, constant osmolality solutions (Nwafor and Coakley, 1985), this condition was well approximated. In each experiment, the membrane potential became more positive, and cell pH, chloride, and water were constant or changed to a minor extent.

Fig. 8 shows five experiments that used this strategy. To examine a full range of membrane potentials, samples with two different starting potentials were prepared. In three experiments (*open symbols*), the starting potential was in the normal (−10 mV) range. In two other experiments (*filled symbols*), cells were placed at very negative membrane potentials by incubation in inosine-pyruvate-phosphate buffer to elevate the cytoplasmic polyanionic compound 2,3-diphosphoglycerate (2,3-DPG) (Deuticke et al., 1971). (Increased nonpermeant cell anion displaced cell chloride, creating a steeper inward chloride gradient and more negative membrane potentials.) Because negative potentials and the strongly buffered external medium forced cytoplasmic acidification, high pH incubations were used to return cell pH to normal (Fig. 8).

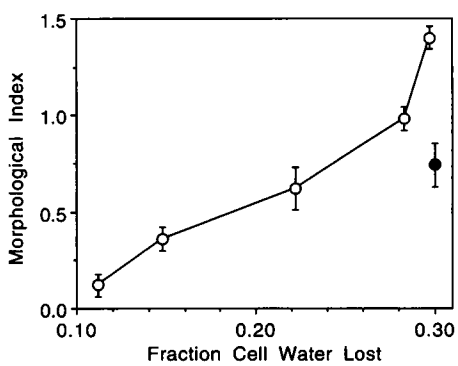

FIGURE 7 Effect of shrinkage on the morphology of positive potential cells in normal pH buffer. Cells were washed and resuspended in 30 mM sodium chloride, 200 mM sucrose, and 5.8 mM sodium phosphate (pH 7.4), and suspension pH was returned to 7.4 with dilute sodium hydroxide. Aliquots were shrunken osmotically by resuspension in the above solution containing additional 200, 250, 300, 350, or 400 mM sucrose (○). A separate aliquot (●) was resuspended at 4°C in the above solution containing 50 μg/mL nystatin (Gedde et al., 1997); after 1 h, nystatin was removed by dilution of the sample in 500 volumes of the same buffer without nystatin. Morphology was assessed and cell volume was assayed by the rapid method (see text).

Over the five experiments, the membrane potential varied from −44 to +47 mV (Fig. 8). Within each experiment, cell pH and cell water remained constant within experimental error (±0.02 units and ±2 pg, respectively; Fig. 8). Cell chloride varied slightly within three experiments (maximum range 26 mM) because of cell chloride leakage in low-chloride solutions (Gedde et al., 1997), and varied within experimental error (±3 mM) in two experiments. In all conditions, red cell morphology remained within the normal discoid range.

We have used 2,3-DPG elevated cells to determine whether negative membrane potentials produce echinocytes. To test whether 2,3-DPG elevated cells are capable of echinocytosis, unfixed 2,3-DPG elevated cells restored to normal cell pH and water were placed on glass surfaces, and the degree of glass crenation was compared to that of normal cells (Fig. 9). The 2,3-DPG elevated cells were fully crenation competent.

Effects of changes in ionic strength

The external ionic strength for samples in Fig. 8 was 40 to 160. Cell chloride concentration varied from 13 to 100 mM (because of 2,3-DPG elevation and cell salt leakage). These ionic strength changes did not displace the morphology from normal (Fig. 8).

DISCUSSION

This study examined the relationship between membrane potential and erythrocyte shape. Although it is known that very large electric fields disrupt membrane integrity (the basis of electroporation techniques), and that physiological membrane potentials influence specialized structures such as voltage-gated ion channels, the effects of physiological potentials on the overall membrane assembly have not been well described. Moderate membrane potentials have been reported to alter human erythrocyte membrane structure, observed as changes in cell shape (Glaser, 1979, 1982). Membrane potential perturbation of this prototypical biological membrane would be of general interest. However, the present study has shown that membrane potential is not a primary determinant of erythrocyte shape.

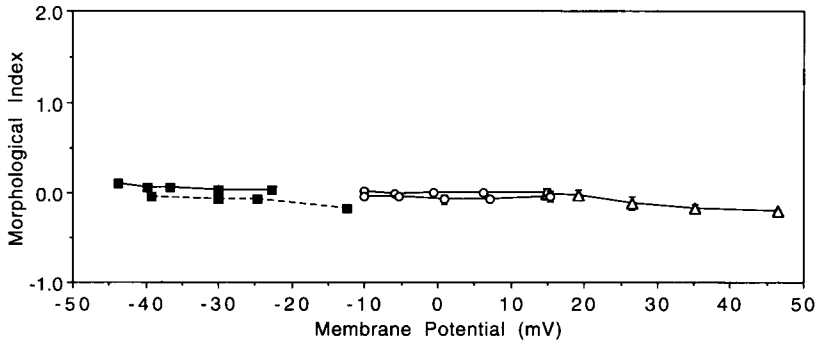

FIGURE 8 Effect of variation in membrane potential on erythrocyte shape. In each of five experiments, cells were suspended in series of unbuffered, reduced chloride solutions, to alter membrane potential while holding other parameters constant (see text). After transfer of cells into buffered solutions designed to preserve the equilibrium state (Materials and Methods), the four physiological parameters plus morphology were assayed. Error bars that are not visible are smaller than the plot symbols. ○, Solutions contained 150, 120, 90, 65, or 40 mM potassium chloride, with sucrose added to maintain osmolality at 270 mosmolal. For the two experiments shown, the mean cell pH was 7.31 ± 0.02; the mean cell water content was 59 ± 1 pg; and cell chloride concentration ranged from 100 to 74 mM (because of chloride leakage; Gedde et al., 1997). △, Solutions contained 50, 40, 30, 20, or 10 mM potassium chloride, with potassium gluconate added to maintain osmolality at 270 mosmolal. The mean cell pH was 7.21 ± 0.02; mean cell water was 64 ± 2 pg; and cell chloride concentration ranged from 91 to 78 mM. ■, Erythrocyte 2,3-diphosphoglycerate was elevated by incubation in IPP buffer. ——, After 2 h of IPP incubation, approximately normal cell pH and water were restored by equilibration in 90 mM potassium chloride and 10 mM HEPES (pH 8.0). Reduced chloride solutions contained 90, 75, 60, 45, or 30 mM potassium chloride, with sucrose added to maintain osmolality at 180 mosmolal. Mean cell pH was 7.04 ± 0.01; mean cell water was 70 ± 2 pg; and mean cell chloride concentration was 13 ± 1 mM. – – –, After 1 h of IPP incubation, normal cell pH and water were restored by equilibration in 100 mM potassium chloride and 20 mM Tris (pH 8.2). Solutions contained 100, 75, 50, or 25 mM potassium chloride, with sucrose and up to 30 mM potassium gluconate added to maintain osmolality at 215 mosmolal. The mean cell pH was 7.26 ± 0.02; the mean cell water was 65 ± 1 pg; and the mean cell chloride concentration was 16 ± 3 mM.

Sources of disparity between earlier and present findings

A key factor in this study was the control of confounding cell properties. Some previous studies attributed pH-induced shape changes in low-chloride buffers to membrane potential shifts, without controlling for changes in other properties such as cell pH and cell water (Glaser, 1979, 1982). Crenation of cells placed in low-chloride solutions at normal pH and permeabilized to cations was attributed to membrane potential shifts, although permeabilization also resulted in severe cell shrinkage (Glaser, 1979; Glaser et al., 1987; Hartmann and Glaser, 1991). An experiment in the present study (Fig. 7) showed that shrinkage, not potential, correlates with shape change in these conditions.

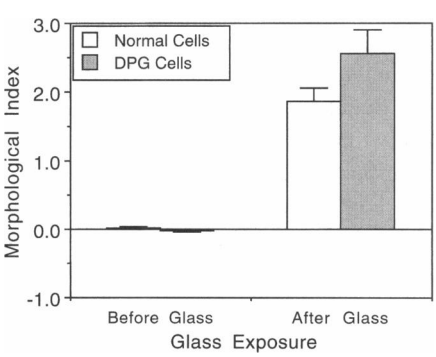

FIGURE 9 Crenation-competence of 2,3-diphosphoglycerate-elevated erythrocytes. Erythrocytes were incubated for 2 h in IPP buffer (Materials and Methods), then equilibrated in 100 mM potassium chloride and 20 mM Tris (pH 8.2) to restore normal cell pH and water. Untreated cells were equilibrated in 140 mM potassium chloride, 20 mM HEPES (pH 7.4). Cell water of the two samples was the same by rapid cell volume assay. Morphology of both samples was assayed; then an unfixed aliquot of each was placed between a glass slide and coverslip, and the morphology of 100 cells was immediately scored (time required: 50–100 s). ■, Untreated cells. ▨, Elevated 2,3-diphosphoglycerate cells.

The effects of these confounding parameters can account for disparities between results of this and previous studies, but other aspects of the earlier studies deserve comment. Morphology observations were made after sedimenting unfixed cells on glass, although glass surfaces are known to crenate unfixed red cells (Trotter, 1956; Weed and Chailley, 1973; and Fig. 9), and the authors acknowledge that glass seemed to have an independent effect on cell shape in some conditions (Glaser et al., 1991). Membrane potentials were calculated from theory rather than measured (Brumen et al., 1979; Glaser and Donath, 1984), but the calculations did not consider cell salt leakage that occurs in low-chloride solutions (Gedde et al., 1997) and are probably not accurate in extremely shrunken cells. Morphology was assessed after ionophore treatment, but ionophores have independent shape effects, as we have found for nystatin (Gedde et al., 1997), and as the authors have noted for valinomycin (Glaser et al., 1991). In the present study these problems were avoided.

A study from another laboratory found that membrane potentials as negative as −80 mV had no discernible effect on erythrocyte shape (Bifano et al., 1984). The experiments employed treatment of red cells with a variety of membrane-active species (DIDS, albumin, diS-C_3(5), valinomy-

cin, FCCP, A23187, and calcium ions) before assessment of cell shape. The study did not investigate shape effects of similarly positive potentials. In contrast, the present study used no membrane-active compounds (apart from glutaraldehyde) in investigating the shape effects of both positive and negative potentials.

Assay of cell properties

This and the following study (Gedde et al., 1997) depended on convenient, accurate assays for morphology and four cell properties (membrane potential, cell pH, cell chloride, and cell water). Because in red cells the chloride gradient determines both membrane potential and the pH gradient, assay of either cell chloride or membrane potential or cell pH allows relatively easy determination of the other two. Determination of the first of the three properties, however, is difficult.

Membrane potential may be assessed by scintillation counting of ^{36}Cl and determination of the chloride distribution (Freedman and Hoffman, 1979), or by measuring the fluorescence of potential-sensitive dyes (Bifano et al., 1984). Accurate determination of the chloride distribution requires complex calculations to correct for the presence of cell solids and trapped supernatant in assayed cell pellets (see Appendix A). Signals from fluorescent dyes must be calibrated with respect to an independent measure of membrane potential, such as the pH gradient. The most powerful assays of cell state use spectroscopic techniques such as nuclear magnetic resonance. Such methods can detail, for example, the dependence of red cell buffering capacity on cell pH (nonlinearity of the plot of cell chloride versus cell pH) (Raftos et al., 1990).

The present study employed direct assay of packed cell lysate pH, with calculation of membrane potential and cell chloride concentration from cell pH, external pH, and external chloride, and gravimetric measurement of cell water. An underlying assumption was that protons were at an equilibrium distribution corresponding to the chloride gradient at the time of measurement. Proton equilibrium as assessed by stability of external pH was confirmed before measurement for each sample. Close agreement of results from the present system and an alternative cell pH assay (Fig. 3) and published titration data (Fig. 4) confirm the validity of this approach. It may be concluded that, relative to spectroscopic methods, this system of assays was as accurate as those used in previous studies (Dalmark, 1975; Freedman and Hoffman, 1979; Bifano et al., 1984), with the advantage of being suited to the analysis of multiple samples.

Assay of morphology received careful consideration. Cells were fixed before observation, the approach used in the classic SEM studies of red cell morphology (Bessis, 1973). Glutaraldehyde fixation prevented the morphology effects of glass slides and provided time for careful quantitation. Because high concentrations of glutaraldehyde can shrink and distort cells before fixation is complete (Hayat, 1981), dilute fixative (0.2%) was used. The fixative vehicle was the experimental supernatant for each sample; thus, cells equilibrated in experimental buffer were transferred to the same buffer carrying a fixing but osmotically insignificant glutaraldehyde concentration. Thus assayed morphology was expected to be identical to prefixation morphology.

Experimental strategy: independent variation of membrane potential

In each experiment shown in Fig. 8, lowering external chloride in constant-osmolality, unbuffered solutions made membrane potential more positive, while cell pH, chloride, and water remained constant. Membrane potential changed with external chloride because red cell potential is determined by chloride distribution. Other properties remained constant because, without external buffering, cell pH was fixed; that is, because of strong cytoplasmic buffering, change in the pH gradient imposed by change in the chloride gradient was accommodated entirely by change in external pH. Cell chloride content depended only on cell pH, so it also remained unchanged. At constant osmolality, cell water was constant, and cell chloride concentration remained unchanged. (In practice, lowered chloride solutions allowed leakage of varying amounts of cell potassium chloride (Gedde et al., 1997).)

Elevation of cell 2,3-DPG created membrane potentials as negative as −45 mV at normal pH, facilitating study of the relationship between membrane potential and shape. This polyanion is thought to increase membrane protein lateral mobility (Schindler et al., 1980) by weakening spectrin's association with actin and band 4.1 (Sheetz and Casaly, 1980, 1981); the effect is greatest above pH 8.0 (Sheetz and Casaly, 1981). Membrane mechanical studies found slight increases in membrane viscosity in the presence of elevated 2,3-DPG (Waugh, 1986; Chasis and Mohandas, 1986; Suzuki et al., 1990), but one study concluded it was "unlikely that 2,3-DPG affects erythrocyte membrane material properties under physiologic conditions" (Waugh, 1986). In no study was a shape effect of 2,3-DPG elevation noted. In this study, 2,3-DPG elevated cells with normal cell pH, water, and potential had normal discoid morphology (Fig. 8) and remained fully crenation competent (Fig. 9). Therefore it seemed appropriate to study the effects of negative membrane potential on shape in these cells.

These experiments demonstrated unambiguously that, when other cell properties remain constant, a broad variation in membrane potential (−45 to +45 mV) does not perturb red cell shape. It follows that one or more of the other changing red cell properties mediates change in membrane curvature and shape in altered external pH. The following study (Gedde et al., 1997) sought to identify the mediating factor.

APPENDIX A

Calculation of membrane potential from ^{36}Cl assay data

In cells with a dominant permeant ion, membrane potential at equilibrium is determined by the ion's activity distribution at equilibrium. The ratio of intracellular to extracellular activities is known as the Donnan ratio, K. Membrane potential is known from K by the Nernst equation

$$\Delta\Psi = -\frac{RT}{zF}\ln \mathbf{K}, \tag{A1}$$

where $\Delta\Psi$ is the potential (V), R is the gas constant (J/mol · K), T is temperature (K), z is ion valence, and F is Faraday's constant (C/mol).

In red cells, chloride is the dominant permeant ion, and the Donnan ratio is the chloride activity (a_{Cl}) ratio. When T = 23°C,

$$\Delta\Psi\ (\text{mV}) = 25.5 \ln\left(\frac{(a_{Cl})_{in}}{(a_{Cl})_{out}}\right). \tag{A2}$$

Because chloride activity (a_{Cl}) equals the chloride activity coefficient (γ_{Cl}) times chloride concentration ([Cl]),

$$\Delta\Psi\ (\text{mV}) = 25.5 \ln\left(\frac{\gamma_{Cl_{in}}}{\gamma_{Cl_{out}}}\right)\left(\frac{[Cl]_{in}}{[Cl]_{out}}\right). \tag{A3}$$

The chloride activity coefficients may be approximated if the chloride extracellular concentration and the chloride concentration ratio are known.

The chloride concentration ratio, commonly termed r_{Cl}, may be determined from equilibrium intracellular and extracellular concentrations of ^{36}Cl:

$$r_{Cl} = \frac{[^{36}Cl]_{in}}{[^{36}Cl]_{out}}. \tag{A4}$$

$[^{36}Cl]_{out}$ is determined easily as ^{36}Cl dpm per volume of suspension supernatant:

$$[^{36}Cl]_{out} = \frac{^{36}Cl_{sup}}{V_{sup}} \tag{A5}$$

Determination of $[^{36}Cl]_{in}$ is less straightforward. In addition to intracellular water, packed cell pellets contain trapped extracellular water and cell solids. Therefore, cell ^{36}Cl dpm equals pellet ^{36}Cl dpm ($^{36}Cl_p$) minus trapped ^{36}Cl dpm ($^{36}Cl_{tw}$), and cell water volume equals pellet volume (V_p) minus cell solids volume (V_{sol}) minus trapped water volume (V_{tw}). Symbolically,

$$[^{36}Cl]_{in} = \frac{(^{36}Cl_p - {}^{36}Cl_{tw})}{(V_p - V_{sol} - V_{tw})}. \tag{A6}$$

In the next two sections, ^{36}Cl assay data are used to calculate the intracellular chloride concentration ($[^{36}Cl]_{in}$) according to Eq. A6 and the chloride ratio (r_{Cl}) according to Eqs. A4 and A5. Then membrane potential is calculated using Eq. A3, and cell pH is determined according to Eq. A1 and the definition of pH.

In the last section, the effects of the described corrections are demonstrated.

Calculation of intracellular concentration of ^{36}Cl

Trapped extracellular ^{36}Cl in a red cell pellet equals the trapped water ^{36}Cl concentration times the volume of trapped water:

$$^{36}Cl_{tw} = ([^{36}Cl]_{out})(V_{tw}). \tag{A7}$$

The volume of trapped extracellular water (V_{tw}) equals the pellet volume (V_p) times the volume fraction of trapped water relative to total pellet volume ($V\text{Fr}_{tw}$, defined as V_{tw}/V_p). $V\text{Fr}_{tw}$ equals the volume fraction of trapped water relative to total pellet water (V_{tw}/V_{pw}) times the volume fraction of total pellet water relative to total pellet volume (V_{pw}/V_p). When water fractions are considered to have densities of 1 g/ml, V_{tw}/V_{pw} equals M_{tw}/M_{pw}, which is $M\text{Fr}_{tw}$, the mass fraction of trapped water relative to pellet water. Likewise, V_{pw}/V_p equals M_{pw}/M_p, which is $M\text{Fr}_{pw}$, the mass fraction of pellet water relative to total pellet mass, times pellet density (ρ_p). Therefore,

$$V_{tw} = (V_p)(\rho_p)(M\text{Fr}_{pw})(M\text{Fr}_{tw}). \tag{A8}$$

$M\text{Fr}_{tw}$ was deduced as described in Appendix B. $M\text{Fr}_{pw}$ was calculated from cell water assay data (Eq. 7). ρ_p was calculated from cell water assay data as follows. Considering that cell pellets are composed of pellet water and pellet solids, and using the definition of density,

$$\rho_p = \frac{M_p}{M_{pw} + (M_{sol}/\rho_{sol})}. \tag{A9}$$

Pellet mass (M_p), pellet water mass (M_{pw}), and pellet solids mass (M_{sol}) were calculated from cell water assay data (Eqs. 4–6). Cell solids density (ρ_{sol}) was calculated from mass fraction of cell water, ($M\text{Fr}_{cw}$) = 0.666 g water/g cells, and volume fraction of cell water, ($V\text{Fr}_{cw}$) = 0.717 g water/ml cells (Freedman and Hoffman, 1979), by

$$\rho_{sol} = \frac{(V\text{Fr}_{cw}/M\text{Fr}_{cw}) - V\text{Fr}_{cw}}{1 - V\text{Fr}_{cw}} = 1.272\ \text{g/ml}. \tag{A10}$$

The volume of cell solids (V_{sol}) equals the pellet volume (V_p) times the volume fraction of solids in the pellet ($V\text{Fr}_{sol}$, defined as V_{sol}/V_p). By the definition of density, $V\text{Fr}_{sol}$ is equivalent to the mass fraction of solids in the pellet ($M\text{Fr}_{sol}$) times the pellet density (ρ_p) divided by the solids density (ρ_{sol}):

$$V_{sol} = (V_p)(M\text{Fr}_{sol})\left(\frac{\rho_p}{1.272\ \text{g/ml}}\right). \tag{A11}$$

Note that $M\text{Fr}_{sol}$ equals $(1 - M\text{Fr}_{pw})$.

Substitution of Eqs. A7, A8, and A11 into Eq. A6, followed by simplification, gives

$$[^{36}Cl]_{in} = \frac{(^{36}Cl_p/V_p) - (^{36}Cl_{sup}/V_{sup})(M\text{Fr}_{pw})(M\text{Fr}_{tw})(\rho_p)}{1 - (M\text{Fr}_{sol})(\rho_p/1.272\ \text{g/ml}) - (M\text{Fr}_{pw})(M\text{Fr}_{tw})(\rho_p)}. \tag{A12}$$

Calculation of the chloride ratio r_{Cl}

r_{Cl} is found by substituting Eqs. A5 and A12 into Eq. A4. When the sample volumes of the supernatant and the pellet are equal, as in the experiments described herein,

$$r_{Cl} = \frac{(^{36}Cl_p) - (^{36}Cl_{sup})(M\text{Fr}_{pw})(M\text{Fr}_{tw})(\rho_p)}{(^{36}Cl_{sup})(1 - (M\text{Fr}_{sol})(\rho_p/1.272\ \text{g/ml}) - (M\text{Fr}_{pw})(M\text{Fr}_{tw})(\rho_p))}. \tag{A13}$$

The form of this equation corresponds to the corrections made: the second term of the numerator corrects for trapped ^{36}Cl, the second term of the denominator for the volume of cell solids, and the third term of the denominator for the volume of trapped supernatant.

Calculation of membrane potential from r_{Cl}

Membrane potential is related to the Donnan ratio according to Eq. A1. Because the Donnan ratio equals the chloride ratio times its activity coefficient ratio,

$$\Delta\Psi(\text{mV}) = 25.5 \ln \mathbf{K} = 25.5 \ln \left(\frac{\gamma_{Cl_{in}}}{\gamma_{Cl_{out}}}\right)(r_{Cl}). \quad \text{(A14)}$$

The chloride activity coefficient γ_{Cl} depends on chloride concentration (Robinson and Stokes, 1965). When intracellular and extracellular chloride concentrations are near physiological, the activity coefficient ratio is effectively 1. However, intracellular and extracellular chloride concentrations in this study differed by up to sevenfold. Therefore, intracellular and extracellular activity coefficients were calculated by using an empirical best fit of published data (Robinson and Stokes, 1965):

$$\gamma Cl = e^{(-1.114[Cl]^{1/2}+1.103[Cl]-0.5624[Cl]^{3/2})} \quad \text{(A15)}$$

with [Cl] in molal. Cell water chloride concentration was found from measured supernatant chloride concentration (Materials and Methods) and $[Cl]_{cw} = [Cl]_s r_{Cl}$. The calculated estimates of γ_{Cl} were substituted into Eq. A14, and membrane potential was calculated.

Calculation of cell pH

For comparison with cell pH measured in freeze-thaw lysates (Fig. 3), cell pH was calculated from external pH and ^{36}Cl assay data by recognizing that the equilibrium proton distribution follows the Donnan ratio K, but is the inverse of the chloride ratio (Eq. A1):

$$\mathbf{K} = \left(\frac{a_{Cl^-_{in}}}{a_{Cl-_{out}}}\right) = \left(\frac{a_{H^+_{out}}}{a_{H^+_{in}}}\right). \quad \text{(A16)}$$

Then, from the definition of pH,

$$pH_{in} = pH_{out} - \log \mathbf{K}, \quad \text{(A17)}$$

where K was determined according to Eq. A14.

Effects of corrections on chloride ratios calculated from ^{36}Cl assay data

To investigate the effects of the corrections for trapped water, trapped dpm, and cell solids, chloride ratios were calculated from ^{36}Cl assay data for a high cell water, positive potential, low cell pH sample; a normal cell water, neutral potential, normal cell pH sample; and a low cell water, negative potential, high cell pH sample (Table 1). As described in the table legend, Eq. A13 was modified to calculate an apparent chloride ratio (no corrections), a corrected chloride ratio (all three corrections), and trapped volume, trapped dpm, and cell solids volume corrected ratios.

For all samples, the corrected chloride ratio was significantly different from the apparent chloride ratio, with differences corresponding to membrane potential differences of +5.8, +8.0, and +5.1 mV for the low, neutral, and high pH samples, respectively. The trapped volume corrected ratio was significantly different from the apparent ratio for all but the low pH sample, with differences corresponding to membrane potential differences of 0.0, +0.5, and +1.2 mV, respectively. The trapped dpm corrected ratio likewise was significantly different from the apparent ratio for all but the low pH sample, corresponding to potential differences of 0.0, −0.8, and −6.4 mV, respectively. The cell solids volume corrected ratio was significantly different from the apparent ratio for all samples, corresponding to membrane potential differences of +5.8, +8.0, and +9.6 mV, respectively.

The effects of the corrections are readily understood. Supernatant trapped in the pellet increases the apparent volume of cell water, which decreases the calculated cell water ^{36}Cl concentration, decreasing the calculated chloride ratio and the membrane potential. Therefore, including the trapped volume correction makes the calculated potential more positive, with the greatest effect in samples with the greatest trapped volume (i.e., shrunken samples). Supernatant ^{36}Cl trapped in the pellet increases calculated cell water ^{36}Cl concentration, increasing calculated membrane potential. The magnitude of the effect depends on both the amount of trapped supernatant and the relative supernatant ^{36}Cl concentration; therefore, the correction is greatest in samples in which supernatant ^{36}Cl concentration is great relative to pellet concentration (i.e., negative potential samples). Cell solids are present in every sample, and their relative volume increases as cell water decreases. Their presence decreases calculated cell water ^{36}Cl concentration, chloride ratio, and membrane potential.

TABLE 1 Effects of corrections for trapped water volume, trapped water dpm, and cell solids volume on calculation of the chloride ratio from ^{36}Cl assay data

Cell state	(1) Apparent chloride ratio	(2) Corrected chloride ratio	(3) Trapped volume corrected ratio	(4) Trapped dpm corrected ratio	(5) Cell solids volume corrected ratio
Swollen (93 pg) + $\Delta\Psi$ (+9.5 mV) Low pH (5.3)	1.203 ± 0.018	1.508 ± 0.022	1.203 ± 0.018	1.203 ± 0.018	1.508 ± 0.022
		$p < 0.01$	NS	NS	$p < 0.01$
Normal size (72 pg) ~ 0 $\Delta\Psi$ (−1.0 mV) Normal pH (7.3)	0.697 ± 0.003	0.955 ± 0.004	0.712 ± 0.003	0.675 ± 0.003	0.956 ± 0.004
		$p < 0.01$	$p < 0.01$	$p < 0.01$	$p < 0.01$
Shrunken (58 pg) − $\Delta\Psi$ (−30 mV) High pH (9.0)	0.218 ± 0.003	0.266 ± 0.005	0.229 ± 0.004	0.170 ± 0.003	0.318 ± 0.005
			$p < 0.01$	$p < 0.01$	$p < 0.01$

Cells were equilibrated in buffers containing 100 mM KCl and 50 mM MES, pH 5.1 (swollen sample), 50 mM HEPES, pH 7.3 (normal size sample), or 50 mM CHES, pH 9.5 (shrunken sample). Supernatant and pellet ^{36}Cl dpm were measured in duplicate for three cell samples. Means ± SD of chloride ratios calculated by five methods for each of the three samples are shown. 1) The apparent chloride ratio assumes that all pellet volume is cell water volume and that all pellet ^{36}Cl is cell water ^{36}Cl, and is calculated as the ratio of the ^{36}Cl dpm found in equal volumes of pellet and supernatant. 2) The corrected chloride ratio is the apparent ratio adjusted for trapped water dpm, trapped water volume, and cell solids volume using cell water assay data, according to Eq. A13. 3) Trapped volume corrected ratio is apparent ratio adjusted for trapped cell water volume only, by including only the trapped volume term in Eq. A13 (omitting trapped dpm and cell solids volume terms). 4) Trapped dpm corrected ratio is apparent ratio adjusted for trapped dpm by including only the trapped dpm term in Eq. A13. 5) The cell solids volume corrected ratio is the apparent ratio adjusted for cell solids volume by including only the cell solids volume term in Eq. A13. p values represent significance levels of the differences between corrected ratios and corresponding apparent ratios. Significance levels were determined using the paired, two-sided t-test. NS, not significant.

Including the correction for cell solids volume increases calculated membrane potential in all samples, with the greatest effects in shrunken cells.

In this study, corrections were necessary to compare cell pH values obtained by ^{36}Cl assay and direct pellet lysate measurement. Are corrections necessary in a routine ^{36}Cl assay of red cell membrane potential? Omission of all corrections gave calculated membrane potentials 5–10 mV more negative than when all corrections were included, so correction should be made when a deviation of this size would affect interpretation of a study. However, the three corrections had different impacts on the final calculated result. The trapped volume and dpm corrections had opposite signs and partly cancelled each other in all samples. Moreover, when the trapped volume is small, as in normally hydrated cells, the combined effect of the two trapping corrections is expected to be negligible. In contrast, the effect on calculated membrane potential of the correction for the presence of cell solids was on the order of 5–10 mV. Thus omission of the cell solids correction is predicted to cause a 5–10-mV inaccuracy in the calculated membrane potential, and correction for cell solids volume alone is a reasonable alternative to full correction of ^{36}Cl assay data.

APPENDIX B

Correction of measured cell water for trapped supernatant

Red cell pellets contain trapped supernatant. If the amount trapped is small and unvarying, it may be ignored without significant error. However, trapping depends on cell hydration: shrunken cells trap significantly more supernatant than normal or swollen cells (McConaghey and Maizels, 1961). Covariance of trapping with the cell properties studied here could skew cell water results and systematically invalidate statistical analysis.

Trapping is commonly estimated using radiolabeled probes (Maizels and Remington, 1959), but because these methods were found to be cumbersome and imprecise, an alternative method was devised. True cell water (cw_{true}) in normal reference cells was found (by subtracting trapped [^{14}C]inulin space from measured cell water (cw_{meas})), and reference cell osmoles (O_c) was calculated from true cell water and external osmolality (Os_{out}). Sample cells were placed at high external osmolalities under conditions in which salt could not enter or leave the cell (cell pH constant and external salt isotonic or greater), so cell salt osmoles could be assumed to be constant. Then, adjusting reference cell osmoles for the increase in hemoglobin osmoles (O_{Hb}) that occurs in shrunken cells, true cell water was predicted from cell osmoles and osmolality for each sample. Comparison of measured cell water to true gave the trapped water fraction. The resulting expression for trapped fraction dependence on measured cell water was used to correct all cell water assay results in this study.

Estimation of trapped water in normal cell pellets

Trapping in pellets of normal cells prepared as in the gravimetric cell water assay (centrifugation at 8800 × *g* for 15 min) was measured using [^{14}C]methoxy-inulin (Sigma) by two methods: directly, by ^{14}C scintillation counting of the pellet; and by dilution, by comparing probe concentration in a supernatant solution before and after dilution into the trapped space. The methods gave 3.5 ± 0.2 and 3.8 ± 0.5% (gram trapped water per gram pellet water), respectively. Because the actual trapped volume may be somewhat greater (Maizels and Remington, 1959), subsequent experiments assumed that 4% of normal cell pellet water was trapped supernatant (that normal $cw_{true} = 0.96\, cw_{meas}$). Substitution of either 3% or 5% for this value resulted in only minor changes in calculated values and had no effect on the conclusions of the study.

Experimental design

Calculation of true cell water in shrunken cells required the assumption that total osmoles in these cells, except for changes in hemoglobin osmoles, was the same as in reference cells. Cell cation leakage was avoided by using external salt concentration no lower than 130 mM (Gedde et al., 1997). (Leakage in low-osmolality solutions prevented detailed examination of trapping in swollen samples.) In addition, it was necessary that cell pH stay constant. This was accomplished by using unbuffered external solutions, so that any potential-associated changes in pH gradient would shift external, not cell, pH.

In two separate experiments, cell samples were equilibrated in 130–250 mM potassium chloride, and cell water and supernatant osmolality were measured.

Determination of reference cell osmoles

Total cell osmoles (O_c) in normal cell water reference samples was determined from $O_c = 0.96(cw_{meas})(Os_{out})$, where Os_{out} is extracellular osmolality. (Because water equilibrates across the membrane, internal and external osmolalities were equal.) Values in the two experiments were 16.9 ± 0.1 and 19.0 ± 0.2 fosmol. Their disparity probably reflects donor variation in cell salt and hemoglobin content (Funder and Wieth, 1966), indicating the importance of self-reference in these experiments.

Expression for O_{Hb} (hemoglobin osmoles)

An expression for hemoglobin osmoles as a function of cell water was derived. Freedman and Hoffman (1979) give the hemoglobin osmotic coefficient (ϕ_{Hb}) dependence on hemoglobin concentration as $\phi_{Hb} = 1 + 0.0645\,[Hb] + 0.0258\,[Hb]^2$, with [Hb] in mmolal. Because $[Hb] = [Hb]_o/w$, where $w = cw/cw_o$, using $[Hb]_o = 7.3$ mmolal and $cw_o = 70$ pg gives $[Hb] = 511/cw$ (mmolal). Then

$$\phi_{Hb} = 1 + \left(\frac{33.0}{cw}\right) + \left(\frac{6740}{cw^2}\right). \quad \text{(B1)}$$

Changing [Hb] units to molal gives $[Hb] = 0.511/cw$. Because cw is in picograms, total Hb = cw [Hb] is in femtomoles, and $O_{Hb} = \phi_{Hb} cw[Hb] = 0.511\phi_{Hb}$ is in femtoosmoles, giving

$$O_{Hb}\,(\text{fosmol}) = 0.511 + \left(\frac{16.9}{cw}\right) + \left(\frac{3440}{cw^2}\right). \quad \text{(B2)}$$

Cell osmoles in shrunken cells: adjustment for Hb osmoles

True cell water for the reference sample and measured cell water for the remaining samples were used in Eq. B2 to calculate hemoglobin osmoles. Preliminary estimates of sample cell osmoles and true cell water were calculated from $O_c = O_{c,\,ref} + (O_{Hb} - O_{Hb,\,ref})$, which adjusted total cell osmoles for the change in hemoglobin osmoles with change in cell water, and

$$cw_{true} = \left(\frac{O_c}{Os_{out}}\right). \quad \text{(B3)}$$

Results of Eq. B3 were applied in Eq. B2, giving new estimates; the iteration was continued to convergence, yielding an estimate of true cell water for each sample.

Expression for trapping

Mass fraction of trapped water ($M\text{Fr}_{tw}$) was calculated from $M\text{Fr}_{tw} = (cw_{meas} - cw_{true})/cw_{meas}$ and plotted against measured cell water (Fig. 10). Linear regression gave

$$M\text{Fr}_{tw} = 0.295 - 0.00352\, cw_{meas}. \quad \text{(B4)}$$

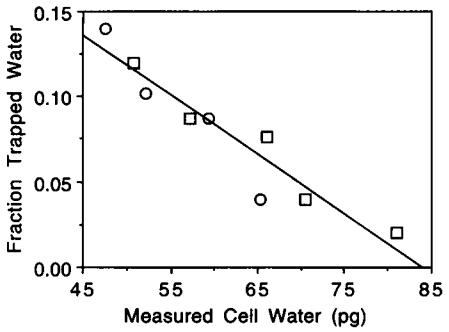

FIGURE 10 Trapped supernatant in the cell water assay. In two separate experiments, normal pH cells were washed and resuspended in unbuffered 130–250 mM potassium chloride solutions (osmolality 0.27–0.45 osmolal). Cell water and osmolality were assayed. Pellet trapping of supernatant was calculated as described in the text. Linear regression gives $y = 0.295 - 0.00352x$.

All cell water results were corrected using this result and $cw_{true} = (1 - MFr_{tw})cw_{meas}$, with trapping assumed to be zero for cell water above 84 pg.

Trapping dependence on shape

Three preliminary experiments investigated the possible effects of cell shape on trapping. No reproducible influence of either stomatocytosis or echinocytosis on trapping was found. Each experiment showed significantly increased trapping in shrunken cells.

REFERENCES

Antonini, E., and M. Brunori. 1975. Hemoglobin and methemoglobin. *In* The Red Blood Cell. D. M. Surgenor, editor. Academic Press, New York. 753–797.

Berk, D. A., R. M. Hochmuth, and R. E. Waugh. 1989. Viscoelastic properties and rheology. *In* Red Blood Cell Membranes: Structure, Function, Clinical Implications. P. Agre and J. C. Parker, editors. M. Dekker, New York. 423–454.

Bessis, M. 1973. Red cell shapes: an illustrated classification and its rationale. *In* Red Cell Shape: Physiology, Pathology, Ultrastructure. M. Bessis, R. I. Weed, and P. F. Leblond, editors. Springer-Verlag, New York. 1–23.

Bessis, M., and M. Prenant. 1972. Topographie de l'apparition des spicules dans les erythrocytes creneles (echinocytes). *Nouv. Rev. Fr. Hematol.* 12:351–364.

Bifano, E. M., T. S. Novak, and J. C. Freedman. 1984. Relationship between the shape and the membrane potential of human red blood cells. *J. Membr. Biol.* 82:1–13.

Brumen, M., R. Glaser, and S. Svetina. 1979. Osmotic states of the red blood cell. *Bioelectrochem. Bioenerg.* 6:227–241.

Bull, B. S. and D. Brailsford. 1989. Red blood cell shape. *In* Red Blood Cell Membranes: Structure, Function, Clinical Implications. P. Agre and J. C. Parker, editors. M. Dekker, New York. 401–421.

Chasis, J. A., and N. Mohandas. 1986. Erythrocyte membrane deformability and stability: two distinct membrane properties that are independently regulated by skeletal protein associations. *J. Cell Biol.* 103: 343–350.

Cook, J. S. 1967. Nonsolvent water in human erythrocytes. *J. Gen. Physiol.* 50:1311–1325.

Daleke, D. L., and W. H. Huestis. 1989. Erythrocyte morphology reflects the transbilayer distribution of incorporated phospholipids. *J. Cell Biol.* 108:1375–1385.

Dalmark, M. 1975. Chloride and water distribution in human red cells. *J. Physiol. (Lond.).* 250:65–84.

Deuticke, B., J. Duhm, and R. Dierkesmann. 1971. Maximal elevation of 2,3-diphosphoglycerate concentrations in human erythrocytes: influence on glycolytic metabolism and intracellular pH. *Pflugers Arch. Eur. J. Physiol.* 326:15–34.

Elgsaeter, A., B. T. Stokke, A. Mikkelsen, and D. Branton. 1986. The molecular basis of erythrocyte shape. *Science.* 234:1217–1223.

Ferrell, J. E., Jr., and W. H. Huestis. 1984. Phosphoinositide metabolism and the morphology of human erythrocytes. *J. Cell Biol.* 98:1992–1998.

Ferrell, J. E., Jr., K.-J. Lee, and W. H. Huestis. 1985. Membrane bilayer balance and erythrocyte shape: a quantitative assessment. *Biochemistry.* 24:2849–2857.

Freedman, J. C., and J. F. Hoffman. 1979. Ionic and osmotic equilibria of human red blood cells treated with nystatin. *J. Gen. Physiol.* 74: 157–185.

Fujii, T., T. Sato, A. Tamura, M. Wakatsuki, and Y. Kanaho. 1979. Shape changes of human erythrocytes induced by various amphipathic drugs acting on the membrane of the intact cells. *Biochem. Pharmacol.* 28: 613–620.

Funder, J., and J. O. Wieth. 1966. Potassium, sodium, and water in normal human red blood cells. *Scand. J. Clin. Lab. Invest.* 18:167–180.

Furchgott, R. F., and E. Ponder. 1940. Disk-sphere transformation in mammalian red cells. II. The nature of the anti-sphering factor. *J. Exp. Biol.* 17:117–127.

Gary Bobo, C. M. 1967. Nonsolvent water in human erythrocytes and hemoglobin solutions. *J. Gen. Physiol.* 50:2547–2564.

Gedde, M. M., D. K. Davis, and W. H. Huestis. 1997. Cytoplasmic pH and human erythrocyte shape. *Biophys. J.* 72:000–000.

Glaser, R. 1979. The shape of red blood cells as a function of membrane potential and temperature. *J. Membr. Biol.* 51:217–228.

Glaser, R. 1982. Echinocyte formation induced by potential changes of human red blood cells. *J. Membr. Biol.* 66:79–85.

Glaser, R., I. Bernhardt, and E. Donath. 1980. The erythrocyte membrane electric field and its functional role. *Bioelectrochem. Bioenerg.* 7:281–290.

Glaser, R., and J. Donath. 1984. Stationary ionic states in human red blood cells. *Bioelectrochem. Bioenerg.* 13:71–83.

Glaser, R., and J. Donath. 1989. Temperature dependent changes in human red blood cells occur only at definite membrane potentials. *Stud. Biophys.* 134:191–194.

Glaser, R., T. Fujii, P. Muller, E. Tamura, and A. Herrmann. 1987. Erythrocyte shape dynamics: influence of electrolyte conditions and membrane potential. *Biomed. Biochim. Acta.* 46:S327–S333.

Glaser, R., C. Gengnagel, and J. Donath. 1988. Membrane electric field and erythrocyte shape. *Stud. Biophys.* 127:201–206.

Glaser, R., C. Gengnagel, and J. Donath. 1991. The influence of valinomycin induced membrane potentials on erythrocyte shape. *Biomed. Biochim. Acta.* 50:869–877.

Hartmann, J., and R. Glaser. 1991. The influence of chlorpromazine on the potential-induced shape change of human erythrocytes. *Biosci. Rep.* 11:213–221.

Hayat, M. A. 1981. Fixation for Electron Microscopy. Academic Press, New York.

Jacobs, M. H., and D. R. Stewart. 1947. Osmotic properties of the erythrocyte. XII. Ionic and osmotic equilibria with a complex external solution. *J. Cell. Comp. Physiol.* 30:79–103.

Jinbu, Y., S. Sato, T. Nakao, M. Nakao, S. Tsukita, S. Tsukita, and H. Ishikawa. 1984. The role of ankyrin in shape and deformability change of human erythrocyte ghosts. *Biochim. Biophys. Acta.* 773:237–245.

Lin, S., E. Yang, and W. H. Huestis. 1994. Relationship of phospholipid distribution to shape change in Ca^{2+}-crenated and recovered human erythrocytes. *Biochemistry.* 33:7337–7344.

Liu, S.-C., and L. H. Derick. 1992. Molecular anatomy of the red blood cell membrane skeleton: structure-function relationships. *Semin. Hematol.* 29:231–243.

Lovrien, R. E., and R. A. Anderson. 1980. Stoichiometry of wheat germ agglutinin as a morphology controlling agent and as a morphology protective agent for the human erythrocyte. *J. Cell Biol.* 58:534–548.

Macey, R. I., J. S. Adorante, and F. W. Orme. 1978. Erythrocyte membrane potentials determined by hydrogen ion distribution. *Biochim. Biophys. Acta.* 512:284–295.

Maizels, M., and M. Remington. 1959. Percentage of intercellular medium in human erythrocytes centrifuged from albumin and other media. *J. Physiol. (Lond.).* 145:658–666.

McConaghey, P. D., and M. Maizels. 1961. The osmotic coefficients of haemoglobin in red cells under varying conditions. *J. Physiol. (Lond.).* 155:28–45.

Morel, F. M. M., R. F. Baker, and H. Wayland. 1971. Quantitation of human red blood cell fixation by glutaraldehyde. *J. Cell Biol.* 48: 91–100.

Nwafor, A., and W. T. Coakley. 1985. Drug-induced shape change in erythrocytes correlates with membrane potential change and is independent of glycocalyx charge. *Biochem. Pharmacol.* 34:3329–3336.

Pfister, H., and H. Pauly. 1964. Membranpotential und Ionenbindung in Proteinlosungen. *Biophysik.* 1:364–369.

Raftos, J. E., B. T. Bulliman, and P. W. Kuchel. 1990. Evaluation of an electrochemical model of erythrocyte pH buffering using ^{31}P nuclear magnetic resonance data. *J. Gen. Physiol.* 95:1183–1204.

Rand, R. P., A. C. Burton, and P. Canham. 1965. Reversible changes in shape of red cells in electrical fields. *Nature.* 205:977–978.

Raval, P. J., D. P. Carter, and G. Fairbanks. 1989. Relationship of hemolysis buffer structure, pH and ionic strength to spontaneous contour smoothing of isolated erythrocyte membranes. *Biochim. Biophys. Acta.* 983:230–240.

Robinson, R. A. and R. H. Stokes. 1965. Electrolyte Solutions: The Measurement and Interpretation of Conductance, Chemical Potential, and Diffusion in Solutions of Simple Electrolytes. Butterworth's, London.

Schindler, M., D. E. Koppel, and M. P. Scheetz. 1980. Modulation of membrane protein lateral mobility by polyphosphates and polyamines. *Proc. Natl. Acad. Sci. USA.* 77:1457–1461.

Schoenfeld, R. G., and C. J. Lewellen. 1964. A colorimetric method for determination of serum chloride. *Clin. Chem.* 10:533–539.

Semplicini, A., A. Spalvins, and M. Canessa. 1989. Kinetics and stoichiometry of the human red cell Na^+/H^+ exchanger. *J. Membr. Biol.* 107:219–228.

Sheetz, M. P., and J. Casaly. 1980. 2,3-Diphosphoglycerate and ATP dissociate erythrocyte membrane skeletons. *J. Biol. Chem.* 255: 9955–9960.

Sheetz, M. P., and J. Casaly. 1981. Phosphate metabolite regulation of spectrin interactions. *Scand. J. Clin. Lab. Invest.* 41:117–122.

Sheetz, M. P., and S. J. Singer. 1974. Biological membranes as bilayer couples: a molecular mechanism of drug-erythrocyte interactions. *Proc. Natl. Acad. Sci. USA.* 71:4457–4461.

Shen, B. W. 1989. Ultrastructure and function of membrane skeleton. *In* Red Blood Cell Membranes: Structure, Function, Clinical Implications. P. Agre and J. C. Parker, editors. M. Dekker, New York. 261–297.

Skoog, D. A. 1985. Principles of Instrumental Analysis. Saunders College Publishing, New York.

Steck, T. L. 1989. Red cell shape. *In* Cell Shape: Determinants, Regulation, and Regulatory Role. W. D. Stein and F. Bronner, editors. Academic Press, San Diego. 205–245.

Suzuki, Y., T. Nakajima, T. Shiga, and N. Maeda. 1990. Influence of 2,3-diphosphoglycerate on the deformability of human erythrocytes. *Biochim. Biophys. Acta.* 1029:85–90.

Trotter, W. D. 1956. The slide-coverslip disc-sphere transformation in mammalian erythrocytes. *Br. J. Haematol.* 2:65–74.

Waugh, R. E. 1986. Effects of 2,3-diphosphoglycerate on the mechanical properties of the erythrocyte membrane. *Blood.* 68:231–238.

Weed, R. I., and B. Chailley. 1973. Calcium-pH interactions in the production of shape change in erythrocytes. *In* Red Cell Shape: Physiology, Pathology, Ultrastructure. M. Bessis, R. I. Weed, and P. F. Leblond, editors. Springer-Verlag, New York. 55–68.

Westcott, C. C. 1978. pH Measurements. Academic Press, New York.

Wolf, A. V., M. G. Brown, and P. G. Prentiss. 1978. Concentrative properties of aqueous solutions: conversion tables. *In* CRC Handbook of Chemistry and Physics. R. C. Weast, editor. CRC Press, West Palm Beach, Florida. D265–D314.